Cellulose (2023) 30:8769–8787
https://doi.org/10.1007/s10570-023-05372-9

ORIGINAL RESEARCH

A green approach for depolymerization of chitosan: applications in hydrogels

Nishat Tabassum · Shoeb Ahmed · Mohammad Muhtasim Ittisaf · Md. Rakid-Ul-Haque · M. Azam Ali

Received: 16 January 2023 / Accepted: 1 July 2023 / Published online: 14 August 2023

Abstract Chitooligosaccharides (COS) are depolymerized chains produced from the natural polymer chitosan and has been determined to exhibit improved biological activities, high solubility in neutral to slightly alkaline pH, because of the lower molecular weight (MW). This makes COS more attractive in biomedical applications. However, earlier studies focused on depolymerization techniques that were either cumbersome or expensive. Here, a convenient two-stage, green synthesis approach was developed and optimized, where gamma irradiation and oxidative degradation with H_2O_2 were used to depolymerize chitosan to produce COS for biomedical applications. The gamma radiation dose level, H_2O_2 degradation reaction's temperature, time and H_2O_2 concentration were varied to obtain the mildest combination of reaction conditions. The most optimum set of conditions (15 kGy, 25°C, overnight reaction with 2% H_2O_2) yielded COS that was soluble in physiological pH range (7–8.5). The COS had a MW of 12.8 ± 1.6 kDa (which was a 95% reduction in MW), a 62.3% degree of deacetylation, and a crystallinity index of 33%. A photopolymerized hydrogel using this COS cross-linked with polyethylene glycol diacrylate (PEGDA) and carboxymethyl cellulose (CMC) was also developed. The hydrogel exhibited high swelling ratio (6.44–10.24), a porous morphology, a compression modulus of 4.5 ± 2.7 kPa (similar to soft tissues), and more than 95% biocompatibility with mammalian cells. This newly developed COS hydrogel involves a simple and green approach for the production of COS and shows promise as a scaffold for artificial soft tissue.

Keywords Chitosan · Chitooligosaccharides · Gamma irradiation · Oxidative degradation · Hydrogel · Depolymerization

Supplementary Information The online version contains supplementary material available at https://doi.org/10.1007/s10570-023-05372-9.

N. Tabassum · S. Ahmed · M. M. Ittisaf · M. Rakid-Ul-Haque
Department of Chemical Engineering, Bangladesh University of Engineering and Technology (BUET), Dhaka 1000, Bangladesh
e-mail: tabassum@mit.edu

S. Ahmed
e-mail: shoebahmed@che.buet.ac.bd

M. M. Ittisaf
e-mail: ittisaf07@gmail.com

M. Rakid-Ul-Haque
e-mail: rakidhaque47@gmail.com

N. Tabassum
Department of Chemical Engineering, Massachusetts Institute of Technology, Cambridge, MA 02139, USA

M. A. Ali (✉)
Centre for Bioengineering and Nanomedicine, Division of Health Sciences, University of Otago, PO Box 56, Dunedin 9054, New Zealand
e-mail: azam.ali@otago.ac.nz

Introduction

Chitosan, despite having strong biological activity, has limited biomedical applications due to its high molecular weight (MW) and lack of solubility in physiological pH conditions. It also forms highly viscous solutions because of its high MW, which makes it difficult to process in pharmaceutical or biomedical formulations. A way to circumvent these issues is to depolymerize chitosan to smaller chain chitooligosaccharides (COS), which have much lower MW that imparts greater solubility and higher biological activity. Usually, COS tend to have MW < 10 kDa and DP < 50–55 (Muanprasat and Chatsudthipong 2017). Some authors consider that chitosan oligomers should only have DP < 10 (Naqvi and Moerschbacher 2017), while others include MW up to 30 kDa as the upper limit (Liaqat and Eltem 2018). This is because true chitosan polymers are considered to have a DP > 100, which is roughly greater than 100 kDa (Naqvi and Moerschbacher 2017). Regardless of the demarcation, COS is characterized by a greater degree of solubility than its precursor, which extends its applicability. COS in place of chitosan has shown stronger anti-inflammatory, anti-tumor and anti-oxidant behavior (Chae et al. 2005; Harish Prashanth and Tharanathan 2007; Muanprasat and Chatsudthipong 2017; Tomida et al. 2009). Complete solubility across a wide range of pH is observed when MW is reduced to below 10 kDa (Mourya, Inamdar, and Choudhari 2011).

Similar to chitosan, COS exhibits various bioactive properties which include antihypertensive, anti-infectious, anti-tumor effects, etc. However, differences in DD, DP, or MW may cause differences in its application (Zou et al. 2016). In its anti-oxidant use, COS can be used to break up the oxidative sequence to prevent cardiovascular diseases. In fact, lower the molecular weight, stronger the anti-oxidative response against an array of radicals such as superoxide, –OH, 2,2-diphenyl-1-picrylhydrazyl (DPPH), etc., with MW < 5 kDa being more promising (Mendis et al. 2007; Mengíbar et al. 2013; Park et al. 2003). Additionally, COS having MW < 3 kDa can suppress the release of cytokines such as inducible nitric oxide synthase (iNOS), tumor necrosis factor (TNF)-α, interleukin (IL)-1β, IL-4 and IL-6 genes that have pro-inflammatory characteristics (Vo et al. 2011; Wu et al. 2015). Also, COS acts as an alleviator to H_2O_2 -induced oxidative stress injury in ECV304 cells (Liu et al. 2009). COS exhibits antimicrobial properties although the extent of this activity varies depending upon the type of chitosan or pH value. It contains primary amino groups which are thought to be the defining factor in its enhancement of antimicrobial properties compared to chitosan (Chen et al. 2002). COS of MW < 2 kDa demonstrated powerful anti-tumor activity against leukemia cells (Kim et al. 2013). COS also reduced the growth of human gastric and breast cancer cells in vitro, by promoting apoptosis and downregulating the expression of growth factors (Jiang et al. 2021; Mallakuntla et al. 2021).

Chitosan and COS are often used in the development of biomimetic materials, such as hydrogels, which are three-dimensional, highly porous networks applicable as artificial tissue scaffolds, wound dressings, drug delivery depots or cell encapsulating systems (Slaughter et al. 2009). Generally, the more hydrophilic the polymers that make up the hydrogel, the greater the swelling under aqueous conditions. This results in better solute transport (Peppas and Reinhart 1983). In fact, a polymer that is water soluble before being cross-linked can be more suitable as a hydrogel base (Ahmed 2015), which makes COS a better alternative to chitosan. For a high percentage of swelling, preparation in an aqueous solution is useful, which also ensures no adverse reactions occur in animal cells (Ahmed 2015; Shorrock and Rees 1988). Additionally, hydrogel formulations can be developed under neutral pH if the precursor material dissolves under such conditions. This can be an important consideration when certain therapeutic proteins such as fibroblast growth factor 20 (FGF20) are to be incorporated into the hydrogel carriers because highly acidic or alkaline pH can denature the protein (Fan et al. 2007).

COS is certainly more useful in biomedical applications, especially in hydrogels. Unfortunately, chitosan depolymerization techniques to produce COS, although many in number, are not convenient. Physical methods involving gamma, UV or microwave radiation, on their own have not been able to sufficiently break down chitosan to soluble COS (Sato et al. 2003). In most cases, drastic conditions such as high temperatures (up to 90°C (Wu et al. 2015) and pressures (Gao et al. 2004; Savitri et al. 2015), or high-intensity doses (Choi et al. 2002; Jin et al. 2017; Muley et al. 2019b), had to be employed. In addition, most studies discovered a limit to the levels up

to which degradation could be achieved. For example, both Muley et al. and Hien et al. reported that gamma radiation at 100 kGy could only achieve a MW reduction of 73–75%, insufficient to achieve the MW of COS. The difficulty in degradation beyond 100 kGy was attributed to the crystalline portions of chitosan (Hai et al. 2003; Muley et al. 2019b). Chemical methods involve either acidic or oxidative degradation. Acidic hydrolysis produces by-products that need to be separated by either fractional precipitation, ultrafiltration or ion exchange (Lin and Lin 2003; Lopatin et al. 2009). Most studies utilized active reactants' concentrations at values typically above 6 M (Cabrera and Van Cutsem 2005; Kabal'Nova et al. 2001; Kazami et al. 2015; Trombotto et al. 2008), and such concentrations can drastically alter the structure of the units and produce toxic by-products (Uchida et al. 1989). Hydrogen peroxide has emerged as an effective depolymerization agent, used mostly in conjunction with radiation. Using H_2O_2, one of the first studies found that chitosan MW decreased by over 95% in the presence of 1.5% H_2O_2 when the reaction temperature was 50°C and duration was 3 h. When the concentration was raised to 3.5%, the same reaction took only 150 min and DP 6–7 COS had the highest yield (Chang et al. 2001). However, peroxide on its own is not as effective, and achieved only limited MW reduction. Najafabadi et al. determined that a reduction of only 22% was possible, even when the peroxide concentration was only 2% (Najafabadi et al. 2018). Hai et al. determined that when 1% H_2O_2 was used to depolymerize chitosan at ambient temperature, COS was produced after 360 h of reaction. Thereafter the reaction stabilized, and the MW did not decrease appreciably as the reaction time continued until 720 h. The MW decreased from 91 to 4.5 kDa (Hai et al. 2019). The major limitation of the enzymatic approach is the cost, as the enzymes are expensive. Also, large batch and column reactors containing immobilized enzymes did not perform satisfactorily in producing enough COS. Downstream purification and separation of the enzymes and products is also expensive. The reaction rate for immobilized enzymes is also lower than that of free enzymes (Kim and Rajapakse 2005).

Most studies have instead focused on simultaneous radiation and oxidative degradation techniques (known as in situ techniques), which have yielded better results as the degradation was faster (Abd El-Rehim et al. 2015; Duy et al. 2011; Hien et al. 2012; Kang et al. 2007; Nguyen et al. 2017; Xuan Du and Xuan Vuong 2019). With such techniques, however it is cumbersome to irradiate large vessels of aqueous samples simultaneously. It is also beneficial to irradiate chitosan in solid form as the number of radicals observed was larger than when the irradiation was carried out in solution (Yoksan et al. 2004). There is a need to develop suitable depolymerization techniques that produce COS conveniently under mild conditions and have fewer processing steps. In this work, we employed a convenient two-stage physicochemical depolymerization process, where gamma irradiation was followed by oxidative degradation with hydrogen peroxide, to produce COS that can dissolve in physiological pH levels. This study therefore focused on finding a strategy to depolymerize chitosan without resorting to simultaneous radiation and oxidative degradation with hydrogen peroxide, which is a cumbersome strategy. This two-stage depolymerization process had not been analyzed in prior studies and we sought to determine a set of optimum conditions for this process. Furthermore, our goal was to employ processing conditions that did not involve high radiation doses, hydrogen peroxide concentrations, and temperatures. As is common with more recent studies, after producing COS, it is necessary to evaluate its effectiveness. Therefore, in this study, a biocompatible hydrogel was successfully prepared under neutral pH to test the feasibility of the COS in biomedical applications. The main outcome of this investigation is thus to establish a COS production technique that can be carried out under mild operating conditions, has scalability potential, and requires minimal processing steps to reduce the bottlenecks in obtaining biomedically relevant COS. Chitosan can thus be depolymerized by avoiding cumbersome in-situ physicochemical processes. The COS produced can then be used to develop biocompatible hydrogels.

Materials and methods

Materials

Chitosan from crab shell chitin was generously supplied by the Biomaterials and Bioengineering Research team from Center of Bioengineering and NanoMedicine (University of Otago, Dunedin, New

Zealand). H_2O_2 (reagent grade, 30%, Merck), lactic acid (reagent grade, 99%, Sigma-Aldrich) and distilled water was used for the chemical depolymerization reaction. NaCl (reagent grade, Merck) was used for the MW tests. Polyethylene glycol diacrylate (PEGDA 700, Merck), Irgacure-2959 and sodium carboxymethyl cellulose (Na-CMC) were used for the hydrogel preparation. A UV radiation chamber (UVB and UVC, average intensity 10 W/m^2) was used for photopolymerization reactions. Glacial acetic acid (99.99%,), Na_2HPO_4, KCl and KH_2PO_4 and dimethylsulfoxide (DMSO) were of reagent grade.

Preparation of irradiated chitosan

Irradiation of chitosan (B_0) was carried out using Co-60 γ-irradiator (present activity 38.6 kCi) at 5, 15, 25, 50, 75 and 100 kGy dose levels. The average measured dose rate was 13.29 kGy/h. Approximately 8 g of chitosan was packaged in a low-density transparent polyethylene bag (3.8 cm by 6.4 cm) and three such packets were then further encased inside a high-density transparent PVC bag for proper exposure to the radiation at room temperature. The samples were placed roughly equidistant from each other, approximately halfway across the PVC bag (Fig. S1) to ensure radiation exposure was the same for all the samples. During irradiation, the bags were placed directly in line with the source and irradiated at room temperature. The irradiated samples were coded B_5, B_{15}, B_{25}, B_{50}, B_{75} and B_{100}, where the subscript denotes the dose applied. The dose levels were proportionate with the time of exposure, with 5 kGy taking 42 min, 15 kGy taking 68 min, 25 kGy taking 113 min, 50 kGy taking 226 min, 75 kGy taking 339 min and 100 kGy taking 451 min.

Depolymerization with hydrogen peroxide

5% (w/v) solutions of the irradiated chitosan were prepared in a solvent containing 1.5% (w/v) of lactic acid and 0–2% (w/v) of hydrogen peroxide (H_2O_2). The reaction vessel was wrapped with aluminum foil to prevent exposure to light. Three different temperatures were tested – 10 ± 2^oC, 25 ± 2^oC and 35 ± 2^oC. 4 h and overnight reaction time periods were chosen. Table 1 shows the experimental parameters that were applied (not in the order in which experiments were performed).

Table 1 Conditions tested in the depolymerization reactions

Experiment no.	Radiation dose (kGy)	Temperature (^oC)	H_2O_2 concentration (% w/v)	Reaction time (h)
1	0	25	2	Overnight
2	5	25	2	Overnight
3	15	25	2	Overnight
4	50	25	2	Overnight
5	100	25	2	Overnight
6	100	25	1	Overnight
7	100	25	2	4
8	100	10	2	Overnight
9	100	35	2	Overnight
10	0	35	2	Overnight
11	0	25	2	4

After the desired time had elapsed, the reaction was quenched with 0.5 M NaOH solution, and the pH was adjusted to approximately 7. Ethanol (96% C_2H_5OH) was used to precipitate the COS produced in the reaction. Centrifugation at 4000 rpm for 15–30 min completely separated the precipitate from the solution, and the precipitate was first heated in 90^{o}C for excess ethanol to boil off and then subsequently dried overnight in an oven at 35^{o}C. The dried COS samples were powdered in the presence of ethanol and then after air-drying for a few minutes, were stored in dry containers for the characterization studies.

COS characterization

At different pH levels, the solubility of the COS samples was analyzed by measuring the transmittance at 600 nm using a UV-Visible spectrophotometer (Hach Spectrophotometer DR 3900). The spectrophotometer was set to transmittance mode at a single wavelength. An optical glass cuvette having a path length of 1 inch was used. A 0.1% (w/v) solution of the COS product obtained from each of the depolymerization reaction mixture was prepared in 1.5% (w/v) lactic acid. The pH was adjusted using 0.5 M NaOH and 1 M lactic acid from 2 to 11. At first, the transmittance of the solvent was measured and set as the baseline. The pH was adjusted at increments of 1 unit and the corresponding transmittance of the COS solution was then measured.

The viscosity average molecular weight (M_v) was determined using the Mark-Houwink-Sakurada relationship $[\eta] = KM_v^{\alpha}$ (1). For chitosan, Wang et al. reported that the values of K and α varied with DD. In the same study, the authors developed a correlation between K and DD ($K = 1.64 \times 10^{-30} DD^{14.0}$ $cm^3.g^{-1}$), as well as for α ($\alpha = -1.02 \times 10^{-2} DD + 1.82$), for a temperature of 30°C (Wang et al. 1991). Using a capillary tube viscometer with a constant temperature water bath (30.0 ± 0.5°C), the viscosity of chitosan, irradiated chitosan and COS samples were determined according to the standard for testing chitosan (ASTM F2103-01) (Zainol, Akil, and Mastor 2009). The capillary had a diameter of 1.2 mm (except in two cases, where 0.8 and 1.5 mm were used). Solutions were prepared using a 0.1 M lactic acid and 0.2 M sodium chloride solvent system (García et al. 2015). Starting with a concentration of 9.6×10^{-3} g/mL, the average fall times for the solution and four dilutions (1.25x, 1.5x, 5x and 10x) were measured. Three triplicate measurements were conducted for each polymer-solvent system. M_v was associated with the number average molecular weight (M_n) using Eq. 1 (Rapado Paneque et al. 2004).

$$M_n = M_v \left[(\alpha + 1) \sqrt{(\alpha + 1)} \right]^{-\frac{1}{\alpha}} \quad (1)$$

For chitosan and COS, a small amount of the powdered samples were pressed against the sample holder and the FTIR (Fourier Transform IR) spectra were recorded using a diamond-tip ATR tool over wavenumbers ranging from 4000 to 400 cm^{-1} at a resolution of 4 cm^{-1} and for a total of 40 scans. The spectra were analyzed to identify key chemical groups. In addition, the DD was determined using the Eq. 3.6 (Brugnerotto et al. 2001). IR spectroscopy is a widely used technique for DD determination (Dong et al. 2001), and is usually determined using the absorption ratios of two bands (A_R/A_M), where A_M is the intensity of a band characteristic to N-acetylation and A_R refers to the intensity of a band that is independent of DD (e.g., –OH, C–, $–CH_2$ or C–O–C bands) using Eq. 2; A_{1320} and A_{1420} represent the absorbances at 1320 (for $–CH_2$) and 1420 cm^{-1} (for amide group), respectively. These two peaks were chosen as they do not vary with changes in humidity.

$$DD(\%) = 100 - \frac{\frac{A_{1320}}{A_{1420}} - 0.03822}{0.03133} \quad (2)$$

XRD analysis was conducted on the Rigaku SmartLab SE, which consisted of a Cu-Kα source (with a nickel filter) and was operated at 40 kV and 30 mA. The wavelength was 1.5 Å, the sweep rate was 1.2 °/min and the scattering angle (2θ) range was 5-60°. From the XRD spectrum, using Bragg's law, the d-spacings for the crystallites in the samples was evaluated, where n is the order of reflection (which is 1), λ is the X-ray wavelength used and θ is the angle of reflection ($d = n\lambda/(2 \sin\theta)$. The crystallinity index was also determined using CI (%)=(I_{20}-I_{16})/I_{20}, where I_{16} represents the intensity at 2θ = 16° and I_{20} is the intensity at 2θ = 20° (Chesnutt et al. 2009).

DSC and TGA analyses of native chitosan (B_0), sample irradiated at 15 kGy (B_{15}) and the optimum COS product (C) were carried out using a Netzsch STA 449F3 instrument under a nitrogen atmosphere (purge flow rate of 20 mL/min). The heating rate was 30°C/min over the range 30-600°C. The DSC-TGA experiments were carried out using 29.9 mg of B_0, 26.3 mg of B_{15} and 15.8 mg of C and the samples were placed in Al_2O_3 pans.

B_0, B_{15} and C were mounted on separate SEM stubs and coated with a 10 nm layer of gold using a mini sputter coater by Quorum Testing. The images were taken at a voltage of 10.0 kV in the EVO 18 SEM machine at two different magnifications. Using SEM images, the surface morphology and texture were visualized.

Hydrogel preparation

To prepare the hydrogel, PEGDA was chosen to form cross-links with COS. It is commonly used as an effective synthetic polymer in biomedical hydrogels, as it is hydrophilic, biocompatible, non-immunogenic, and does not adsorb proteins that could cause fouling or pore blockages in the hydrogel (Slaughter et al. 2009). In fact, PEGDA hydrogels have been widely used in tissue engineering applications as it does not induce any unwanted reactions in cells (Lin et al. 2020; Morris et al. 2017). The small chains of COS however cannot be efficiently cross-linked with PEGDA, and the COS-PEGDA hydrogel solution was found to have a watery consistency. To increase the

viscosity, CMC was used as a thickener, which forms a poly-ionic complex with COS, holding the chains in place for effective binding with PEGDA. CMC itself has high binding and superabsorbent characteristics (Capanema et al. 2018; Fekete et al. 2017).

0.5 g of the COS product was dissolved in 100 mL of 1% (v/v) acetic acid solution and the pH was adjusted to ~7. After overnight stirring, this neutral stock solution was used for the purposes of preparing the COS hydrogel. To 1 mL of this solution, 5 mL of a copolymer solution containing 7.5% (w/v) PEGDA and varying CMC concentration (2 and 4% (w/v) was added. Irgacure 2959, a photoinitiator, was dissolved to make a 1% (w/v) solution in DMSO; from this stock solution, 137 µL was used in the hydrogel formulation such that photocuring required a concentration of 0.02% (w/v) of Irgacure 2959. These low concentrations ensure that the photo-initiator does not induce any toxic effects (Morris et al. 2017). The hydrogel blends were coded COSPCMC-2 and COSPCMC-4 to denote the CMC concentration. Curing was performed under a UVB-UVC combination light source (100–480 nm, 10 W). The curing time (~2 h) was chosen so that both types of hydrogels would be cured simultaneously but the exposure would not be too high. Cylindrical hydrogel specimens of 1 cm by 1 cm were prepared for the characterization studies.

Hydrogel characterization studies

Swelling characteristics

Cylindrically shaped gels were freeze dried and weighed (m_o). The hydrogel samples were then incubated in a PBS solution (pH ~ 7) for 24 h at 37°C. After incubation, the samples were reweighed (m_1) after blotting off the excess surface water using a filter paper. The equilibrium swelling ratio is given by $SR = (m_1\text{-}m_o)/m_1$.

Morphological analysis

Hydrogel samples were cut into thin slices (5 mm thickness) before freeze drying. The gel cross-sections were mounted on SEM stubs and sputter coated with a 10 nm layer of gold for 90 s. Images were obtained at a voltage of 5 kV. Pore structure and surface properties were analyzed using an EVO18 SEM (Carl Zeiss).

Functional group analysis

To assess the cross-linking performance effectively, it is necessary to determine the type of functional groups present in the hydrogels. As such, the IR spectra of the hydrogels were recorded. Freeze-dried samples of the gel were cut into small pieces and then analyzed using a diamond-tip ATR tool over wavenumbers ranging from 4000 to 400 cm^{-1} at a resolution of 4 cm^{-1} and for a total of 64 scans.

Cytotoxicity tests

Although washing and dialysis remove unreacted chemicals from the COS hydrogel, if it is designed to degrade inside the body (such as drug delivery depots or artificial scaffolds that should eventually be replaced by new tissues generated in the body), the chemicals would enter the system. As a result, a cell assay study principally measures the cytotoxicity of any leach-out products in addition to the gel itself is necessary. At first, samples of hydrogel samples of various masses (25 mg, 50 mg and 100 mg) were incubated at 37°C in 10 mLs of PBS solution (pH 7) for the compounds to leach out. The solutions were then filtered through a 0.22-micron syringe filter to sterilize the solutions. To conduct the cytotoxicity analysis, a non-cancer mammalian Vero cell line (kidney epithelial cell lines) extracted from the African green monkey, was incubated in DMEM (Dulbecco's Modified Eagles' medium) containing 1% penicillin-streptomycin (1:1), 0.2% gentamycin and 10% fetal bovine serum (FBS). Cells (3.0×10^4/200 µL) were seeded into a 48-well plate and incubated at 37°C and 5% CO_2. After 24 h, 50 µL sample (sterilized using a 0.22-micron syringe filter) was added to each well. Cytotoxicity was examined under an inverted light microscope after 48 h of incubation. The results were based on n = 2 duplicate samples.

Mechanical tests

A universal testing machine (UTM) by TestResources (100 series) was used to conduct uniaxial compression tests at a displacement rate of 10.00 mm/min on swollen samples measuring an average of Ø 9 mm

by 5 mm (n = 3 samples). Force applied and position were recorded, which were used to evaluate the compressive stress ($\sigma = F/A$) applied and the elastic modulus determined using $\sigma = E(\lambda - \lambda^{-2})$, where σ is the applied stress in Pa/m^2, F is the measured force, A is the cross-section area and λ is the relative deformation of the sample ($\lambda = 1 + /L$), and ε is the deformation and L is the thickness of the sample.

Results and discussion

Optimization of COS production technique

By measuring the UV transmittance of the solutions of chitosan and COS obtained after radiative and oxidative degradation, the extent of solubility at various pH conditions was determined. Chitosan, and by extension the derivatives, exhibit solubility at pH < 5. This is expected, since the primary -NH_2 groups present in the molecule are protonated at such conditions. The defining criteria of solubility at any pH was a transmittance of > 90%, which signaled that no precipitation had occurred, and a clear solution persisted (Zainol et al. 2009). Figure 1 summarizes the optimization studies that were conducted to determine the most optimum temperature, reaction time, hydrogen peroxide concentration and radiation dose that could yield COS of the highest solubility at pH 7–8, which is the physiological pH range. All peroxide reaction tests were conducted on chitosan samples that had been first irradiated at 100 kGy. It is to be noted that solubility tests are conducted in controlled pH conditions instead of pure water as ionic strength of the solution appeared to be a factor governing solubility (Nguyen et al. 2017).

The most optimum combination of peroxide reaction conditions were 25°C, overnight reaction with 2% H_2O_2. The minimum radiation dose that would be required was then determined by performing oxidative degradation at these optimized conditions for chitosan that had been irradiated at various gamma radiation doses. Again, the transmittance was measured at a range of pH values (Fig. 1d). C_o (chitosan without irradiation but degraded with H_2O_2) precipitated out at pH > 6 as demonstrated by the drop in solution transmittance to 84%, while C_1 (5 kGy irradiation) remained soluble up to pH 7.6. C_2 to C_4 (15–100 kGy dose) exhibited transmittance of > 90% beyond pH 7 and up to pH 10, as no precipitation was observed. This is likely due to the fact that as the radiation dose was increased, the chitosan depolymerization progressed further (Hai et al. 2003). Thus, for C_2–C_4, the irradiated chitosan was sufficiently depolymerized, degrading to soluble COS after oxidative treatment with hydrogen peroxide. The radiation plays a significant role in aiding the oxidative degradation; studies by Qin et al. and Kabal'nova et al. showed that such dramatic depolymerization required either

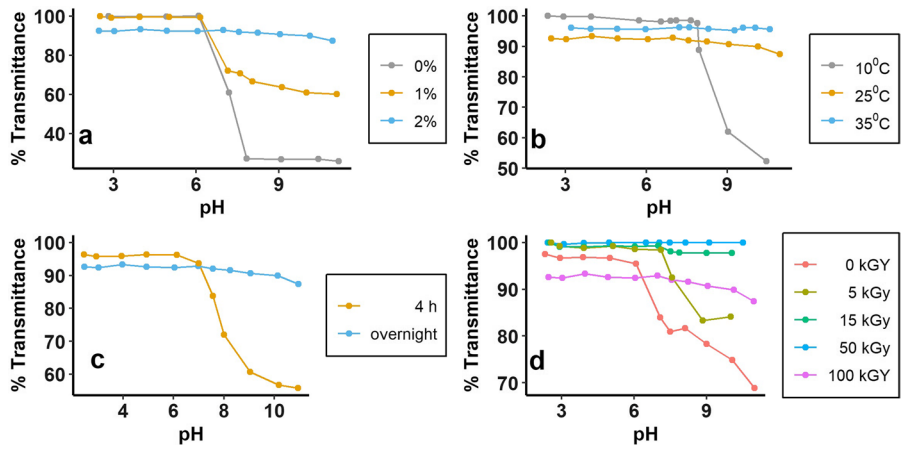

Fig. 1 Transmittance of COS solutions at various pH values showing extent of solubility. Optimization of reaction conditions; **a** impact of hydrogen peroxide concentration (other conditions: 100 kGy irradiation, H_2O_2 reaction conditions (25°C, overnight); **b** the impact of temperature (other conditions: 100 kGy irradiation, H_2O_2 reaction conditions (2% H_2O_2, overnight), **c** impact of reaction time (other conditions: 100 kGy irradiation, H_2O_2 reaction conditions (2% H_2O_2, 25°C), and **d** impact of radiation dose (H_2O_2 reaction conditions (2% H_2O_2, 25°C, overnight reaction))

temperatures above 50°C or hydrogen peroxide concentrations above 0.6 M.

The mechanism of both radiation breakdown and oxidative degradation have been summarized by other authors. The succeeding mechanism for the gamma radiation breakdown has been proposed by Hai and coauthors (Hai et al. 2003). Reaction (i) occurs as the energy of the gamma rays is sufficient to break down a C-H bond in chitosan. The H free radical attacks chitosan chain in the chain propagation reaction (ii), and a free radical is produced on any of the C atoms of the glucopyranose ring. If the free radical center is on C1 or C4, fragmentation of the chains takes place. The glucosamine groups can also participate and break down into ammonia. In the mechanisms below, R–H and R–NH_2 are chitosan chains, $R^{\bullet}(C_n)$ is a chitosan radical, where the unpaired electron is on the C_n atom and F_1 and F_2 are fragments formed after chain scission.

$$R - H \rightarrow R\bullet\left(C_4 - C_6\right) + H\bullet \quad \text{(i)}$$

$$R - H \rightarrow H\bullet \rightarrow R\bullet\left(C_1 - C_6\right) + H_2 \quad \text{(ii)}$$

$$R\bullet\left(C_1, C_4\right) \rightarrow F_1\bullet + F_2(\text{fragmentation}) \quad \text{(iii)}$$

$$R\bullet\left(C_1, C_4\right) \rightarrow F_1\bullet + F_2 \quad \text{(iv)}$$

$$R - NH_2 + H\bullet \rightarrow R\bullet\left(C_2\right) + NH_3 \quad \text{(v)}$$

During oxidative degradation with H_2O_2, the acidic pH of the solution in which the reaction is carried out, causes the unstable H_2O_2 to form H + and HOO- ions that eventually decompose to HO•, O_{2-}• and H_2O. The HO• attacks the chitosan chain, forming free radicals as shown in the previous mechanism (reaction (ii)), except free radical centers on C1, C4 and C5 can lead to fragmentation and hydrolysis reactions, both of which lead to chain breakage.

$$H_2O_2 \leftrightarrow H^+ + HOO^- \quad \text{(vi)}$$

$$HOO^- \rightarrow OH^- + O\bullet \quad \text{(vii)}$$

$$H_2O_2 + PHOO^- \rightarrow HO\bullet + O^{\bullet}{}_{2-} + H_2O \quad \text{(viii)}$$

$$R\text{-}H + HO \rightarrow R\left(C_1 - C_6\right) + H_2O \quad \text{(ix)}$$

$$R\left(C_1, C_4, C_5\right) \rightarrow F_1 + F_2(\text{fragmentation}) \quad \text{(x)}$$

The summary of the optimization studies is given in S1, where the average transmittance values at physiological pH levels 7–8 have been highlighted to show extent of COS solubility at those pH values.

Molecular weight

Prior studies have shown that increase in gamma radiation dose reduces molecular weights as the chain breakdown occurs more rapidly and to a greater extent (Hai et al. 2003; Yoksan et al. 2004; Zainol et al. 2009). Figure 2 shows that in this study, a similar trend was observed. Irradiation at 15 kGy reduced the MW only slightly (by only 3%). From 15 to 50 kGy, the decrease was rapid. The average molecular weight after irradiation at 75 kGy was 86.8 kDa,

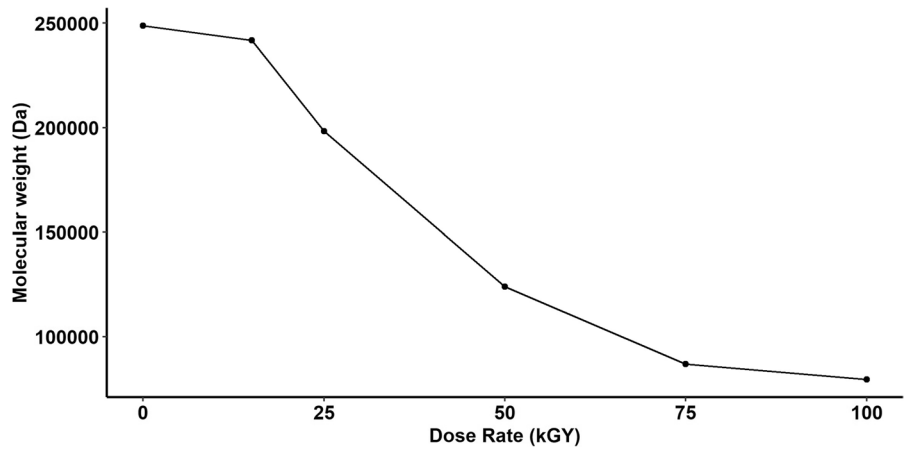

Fig. 2 Effect of radiation on the molecular weight of chitosan (irradiation occurred at room temperature in the presence of air)

which decreased to 79.6 kDa for 100 kGy, which is only an 8% change. This suggests that increasing the dose rate any further would not cause sufficient breakdown of chitosan. An explanation for this breakdown limit was proposed by Yoksan et al.; irradiation only resulted in breakdown of the amorphous regions, while the crystalline portion remained intact. This implies that higher radiation doses cannot produce chitooligosaccharides (COS) of molecular weights < 30 kDa, since the crystalline structure cannot be degraded by radical chain scission reactions (Yoksan et al. 2004). Zainol et al. also confirmed that the MW of chitosan having an initial MW of 576 kDa decreased to 458 kDa at 10 kGy, 242 kDa at 25 kGy, 159 kDa at 50 kGy and finally to 106 kDa at 100 kGy. The correlation graphs are given in supplementary materials (S2).

Similar viscosimetric measurements were carried out for the COS produced after irradiation at 15 kGy and degraded overnight using 2% hydrogen peroxide at 25°C (product C) and an average molecular weight of 12.8 kDa was obtained, a reduction of 95% from the molecular weight of the irradiated precursor (Table 2). Although the most significant molecular weight reduction occurred during the peroxide treatment, these changes required mild conditions. This would not have been possible without prior radiation treatment; Hai et al. treated chitosan having a molecular wight of 36.5 kDa with 2% hydrogen peroxide and determined that although a 93% reduction in molecular weight was possible, it took 720 h (Hai et al. 2019). In another study, a 90 to 70 kDa reduction in molecular weight required 12 h when only 1% H_2O_2 was used (Hien et al. 2012). It can be speculated that the initial radiation treatment sufficiently degraded the amorphous regions and afterwards the H_2O_2 could act more efficiently. Based on the results of solubility and MW, this COS product (C) was chosen to be the most suitable for subsequent characterization and application studies.

FTIR analysis

Table 2 shows the variation in DD after irradiation at different doses and of the optimized product. Because the values of DD are comparable, it can be concluded that neither radiation nor H_2O_2 increased the number of carbonyl groups (C = O), which would have increased DD. Therefore, the functional groups remain intact in these processes. Although previous studies have also concluded that irradiation has no impact on DD (García et al. 2015; Nguyen et al. 2017; Zainol et al. 2009), H_2O_2 has been observed to increase the DD to a much higher degree, as it modified the chemical structure (Nguyen et al. 2017; Qin et al. 2002). Our results however demonstrate that H_2O_2 did not have such a drastic impact (DD of C is 62.3%, whereas for B_0, it is 65.5). This indicates that only the polysaccharide backbone of the chitosan chain participates in the depolymerization reactions, while the functional groups remain intact (García et al. 2015; Zainol, Akil, and Mastor 2009). Yoksan et al. proposed that the DD can remain unaltered if $\bullet COCH_3$ radicals are not formed during scission. The results exhibited in our experiments are in agreement with Yoksan et al.'s findings [48].

The FTIR spectra of B_0, B_{15} and C show almost similar characteristic peaks (Fig. 3a). All spectra show the broad peak for −OH at 3320 cm^{-1}, the narrow band for C=O (amide I) at 1630–1640 cm^{-1}, the characteristic peak for $-NH_2$ at 1570–1590 cm^{-1}. The peak at 1029–1069 cm^{-1} arise due to the stretching vibration of C−O in the C−O−C bond, while that at 1148 cm^{-1} is associated with C–O–H bond

Table 2 Average MW (± standard deviation, n = 3 samples), DD, CI and d-spacings of chitosan, irradiated chitosan and COS

Sample	Number average MW (kDa)	Degree of deacetylation, DD (%)	Crystallinity Index (%)	d-spacing (Å)	
				Form I	Form II
B_0	249 (± 3.5)	65.5	51	7.55	4.24
B_{15}	242 (± 0.6)	65.5	48	7.24	4.17
B_{25}	228 (± 6.3)	65.0	52	–	–
B_{50}	143 (± 25)	65.2	49	–	–
B_{75}	89 (± 10)	65.1	–	–	–
B_{100}	92 (± 24)	64.7	45	–	–
C	12.8 (± 1.6)	62.3	33	–	4.36

– Indicates data not measured

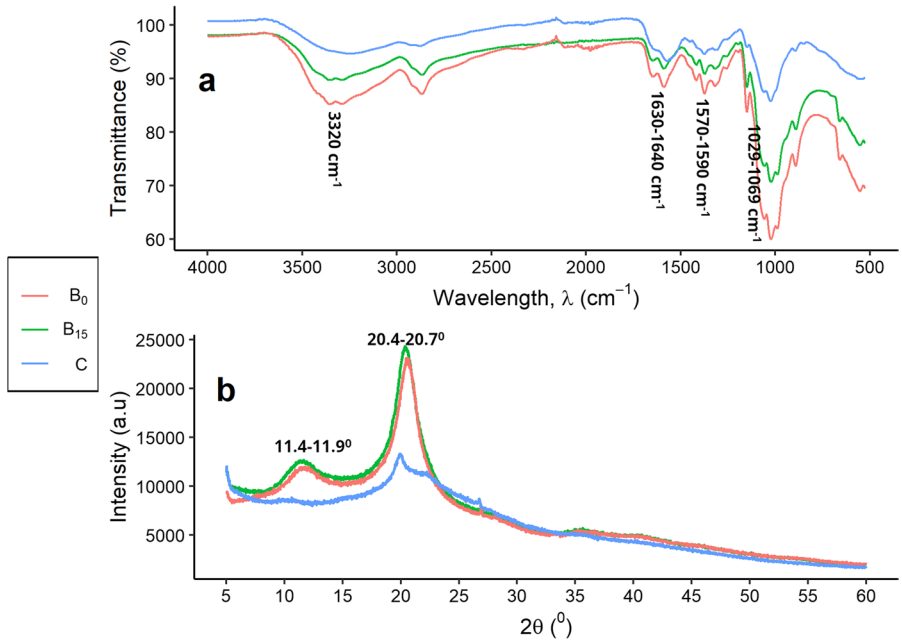

Fig. 3 **a** Comparison between the FTIR spectra of B_0, B_{15} and C, highlighting only the major characteristic peaks; **b** XRD spectra of B_0, B_{15} and C (a.u.: arbitrary units), showing that the peak at 11.4–11.9o has disappeared for C

stretching (Bernardino-Nicanor et al. 2017; Muley et al. 2019). The peak at 885–890 cm^{-1} corresponds to the glucopyranose ring (Yoksan et al. 2004). In other words, the backbone structure did not change significantly. All peaks have been normalized to the same baseline after automatic baseline correction. However, peak analysis revealed slight differences. According to the peak absorption ratio comparison method outlined by Zainol et al. (S3), the ratio between the C=O and –OH absorption peaks differed between the three types of samples. Referring to Fig. S3, the e-f peak height is a measure of the C=O bond and b-c measures the –OH group. The ratio for B_0 was determined to be 0.504, whereas for B_{15} and C, it increased to 0.635 and 0.782 respectively. This is because B_0 had more –OH groups than the others (Muley et al. 2009), while more C=O bonds formed after the chain scission reactions and oxidative degradation of chitosan, which resulted in a slight decrease in DD as shown on Table 2 (Zainol et al. 2009).

XRD analysis

Values of the crystallinity index describe whether the irradiation and oxidative treatment had any impact on the crystalline regions of the samples. The CI of chitosan and the irradiated samples are similar (Table 2), which indicates that irradiation could not sufficiently induce radical chain scission in the crystalline regions; the depolymerization only occurred in the amorphous zones. However, treatment with hydrogen peroxide led to a more drastic reduction, as H_2O_2 greatly accelerates radical formation.

Samuels identified two forms of chitosan. Both are extended 2-fold helix structures and form I has a distinctly sharp characteristic peak at $2\theta = 11^o$, while the one for form II, mostly appears at $2\theta = 20.5^o$ (Samuels 1981). Both B_0 and B_{15} show the first peak respectively at 11.4^o and 11.9^o, and the second one at 20.4^o and 20.7^o (Fig. 3b), with the form II peak being more prominent. This indicates that the radiation scission had minimal impact on the crystalline portion, which also explains why the crystallinity index decreased only slightly (Table 2) (Muley et al. 2019). In form II crystals, the main chain is constrained due to the H bonds, which maintains the packing structure of chitosan (Fan et al. 2009; Yoksan et al. 2004). After the oxidative treatment, a dramatic decrease in crystallinity occurred (C). The peak at 11^o disappeared, while the form II peak diminished in intensity and shifted to 19.8^o. This behavior is consistent with the XRD patterns of tendon hydrated water-soluble COS found in other studies (Fan et al. 2009; Hai et al. 2019). The decrease in the angle reflects the expansion of the crystal lattice due to the formation of a greater number of acetyl groups after depolymerization

(characterized by the lower DD), which is also confirmed by the larger d-spacing (Table 2). Chitosan depolymerization first proceeds in the amorphous region that covers its surface. Once the surface has been sufficiently degraded, the crystalline regions can then be attacked. It is possible that irradiation first depolymerized only the amorphous regions without much impact on the crystal structure. Afterwards, the H_2O_2 could affect the crystalline regions (F. Tian et al. 2003). D-spacings of the crystalline forms found in the B_0, B_{15} and C are summarized in Table 2.

DSC-TGA analyses

Figure 4a shows the TGA behavior of B_0, B_{15} and C, alongside the derivative of the mass loss. All three exhibit two distinct decomposition events. The first event, corresponding to the loss of hydrogen bonded water molecules, occurred at 53.7°C, 49.6°C and 38.0°C respectively. For B_0, the mass loss was 8.6%, B_{15} and C exhibited a loss of 3.1% and 4.3%. The second decomposition was observed at 233.6°C, 234.6°C and 163°C respectively, corresponding to a 31.6%, 43.8% and 45.1% decrease, and occurred when the saccharide rings of the molecules underwent complete degradation (García et al. 2015). The progressive decrease in the decomposition temperatures is due to the decrease in the thermal stability that occurred after the depolymerization reactions (and the decrease in crystallinity) (Timur and Paşa 2018). It is evident from the dramatic differences shown by C that the depolymerization was more severe after irradiation and oxidative degradation by peroxide (Qin et al. 2002). The TGA derivative curve in Fig. 4b correspond to the derivatives of the TGA data in Fig. 4a and confirm the temperatures at which these major mass changes occurred.

The DSC thermograms (Fig. 4c) of the three molecules are similar to the characteristic thermograms of chitosan (García et al. 2015; Kittur et al. 2002; Muley et al. 2019a). The first broad endothermic peaks occurred due to moisture loss, occurring at 109°C for both B_0 and B_{15}, but at 113°C for C. Depending on the structure of the polysaccharide, the water retention capacity changes; the increase in the first endothermic peak's area is associated with the ability to bind more water. Due to depolymerization, the structure became more disordered, which has been correlated with the increase in water retention capacity (Kittur et al. 2002). Decomposition events (breakdown of the amine groups) are depicted by the prominent exothermic peaks, which are observed at around 299°C for B_0 and B_{15} and at 303°C for C. Additionally, the peak height for C is 1.29 mW/mg, an almost 50% reduction than those for B_0 (2.53 mW/g) and B_{15} (2.23 mW/g), indicating that C decomposed more easily.

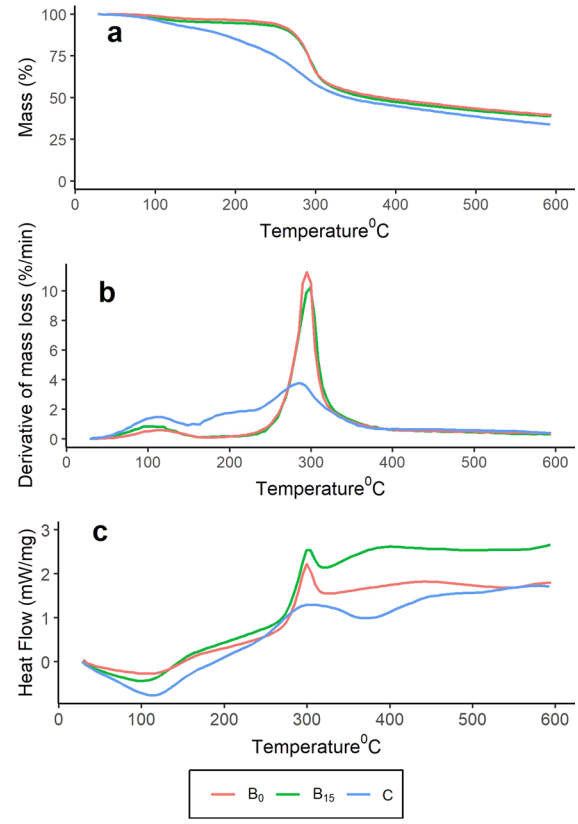

Fig. 4 **a** Thermal degradation behavior of B_0, B_{15} and C; **b** Evaluated values of derivative weights from the TGA data showing regions of major weight loss; **c** DSC thermograms showing phase changes in B_0, B_{15} and C

Morphological characteristics

The SEM analyses (Fig. 5) confirm that major structural changes arose due to the depolymerization. B_0 and B_{15} had a more amorphous structure, characterized by a nonporous texture. Noticeable cracks and fractures appeared on C, including micropores. The fact that B_0 and B_{15} were both viewed on a scale of 10 micron, whereas C could only be resolved at a scale

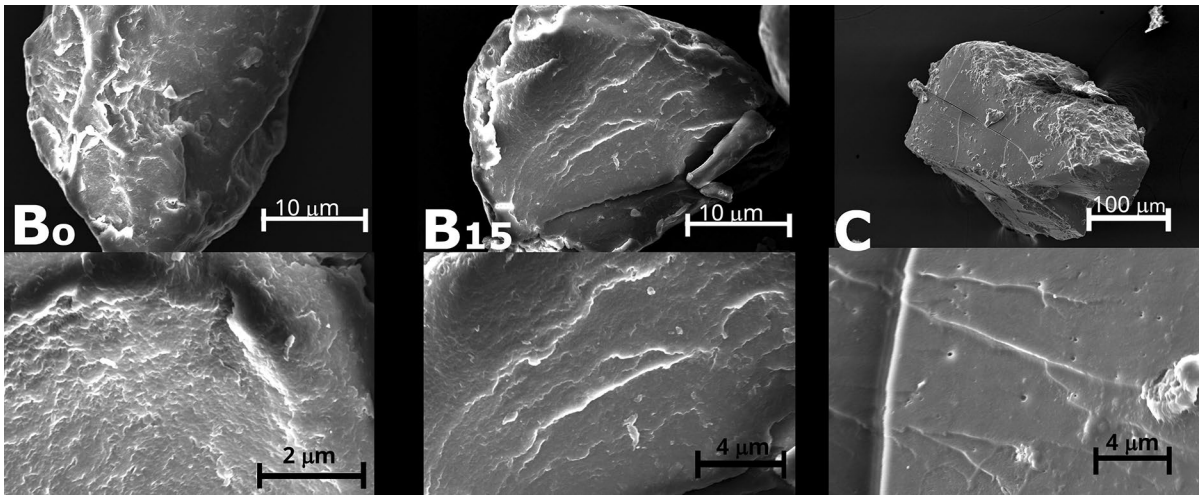

Fig. 5 SEM images showing surface morphology of B_0, B_{15} and C (first row of images at 5 kX, 10 kX and 1 kX magnifications respectively; second magnification at 30 kX, 20 kX and 20 kX respectively)

of 100 micron, indicated that particles of C were much smaller than those of B_0 and B_{15}.

Synthesis of COS-PEGDA-CMC hydrogel

In this study, to make COS-based hydrogels, COS was first mixed with only poly-ethylene glycol diacrylate (PEGDA). Incorporation of PEGDA has been shown to improve mechanical strength of chitosan/COS hydrogels (Jung and Yi 2012). However, as COS had shorter chains (which explains the lower molecular weight), the extent of crosslinking was negligible during the time the polymerization reaction was allowed to proceed (~2 h). The condition that the reaction should occur within a reasonable duration was imposed to avoid long operation times that might be damaging to cell-laden hydrogels. Because of the watery consistency of the COS-PEGDA blend, it was decided that carboxymethyl cellulose (CMC) would be used as a thickener and an additional complexing agent. Using the two individual reactions between CMC-PEGDA, and PEGDA-COS, a possible reaction mechanism can be postulated (Fig. 6). At first, when COS was added to the CMC-PEGDA solution, the small positively charged chains of COS were electrostatically attracted to the negative domains of CMC (Fig. 6A), forming a self-assembling poly-ionic complex (Zhu et al. 2021). Under aqueous conditions, PEGDA does not crosslink with CMC or COS to any appreciable extent. Subsequent photopolymerization resulted in free radical formation on both COS and PEGDA (Fig. 6B), leading to crosslinking between these chains, in addition to cross-linking between PEGDA chains themselves. Such extensive networks resulted in gelation and formation of a cross-linked polymeric complex (Fig. 6C). As the COS chains are smaller, by being attracted to the long CMC chains, COS fragments became organized, which allowed ease of interaction with PEGDA.

Physical characterization of COS-PEGDA-CMC hydrogel

Swelling ratio

After freeze drying, the two different COS-PEGDA-CMC (COSPCMC) hydrogels containing varied concentrations of CMC (2% and 4%), were incubated for 24 h at 37°C in PBS and the swelling behavior was analyzed. For COSPCMC-2 and COSPCMC-4, the ratios were 6.44 and 10.24 (average of n = 3 samples) respectively. The increase in swelling ratios are likely due to the presence of a greater number of COO- groups in a more concentrated solution of CMC, which caused the chains to stiffen and allowed better uptake of water (Barbucci et al. 2000; Reeves et al. 2010). High swelling ratios are associated with the water solubility and hydrophilicity of the precursor

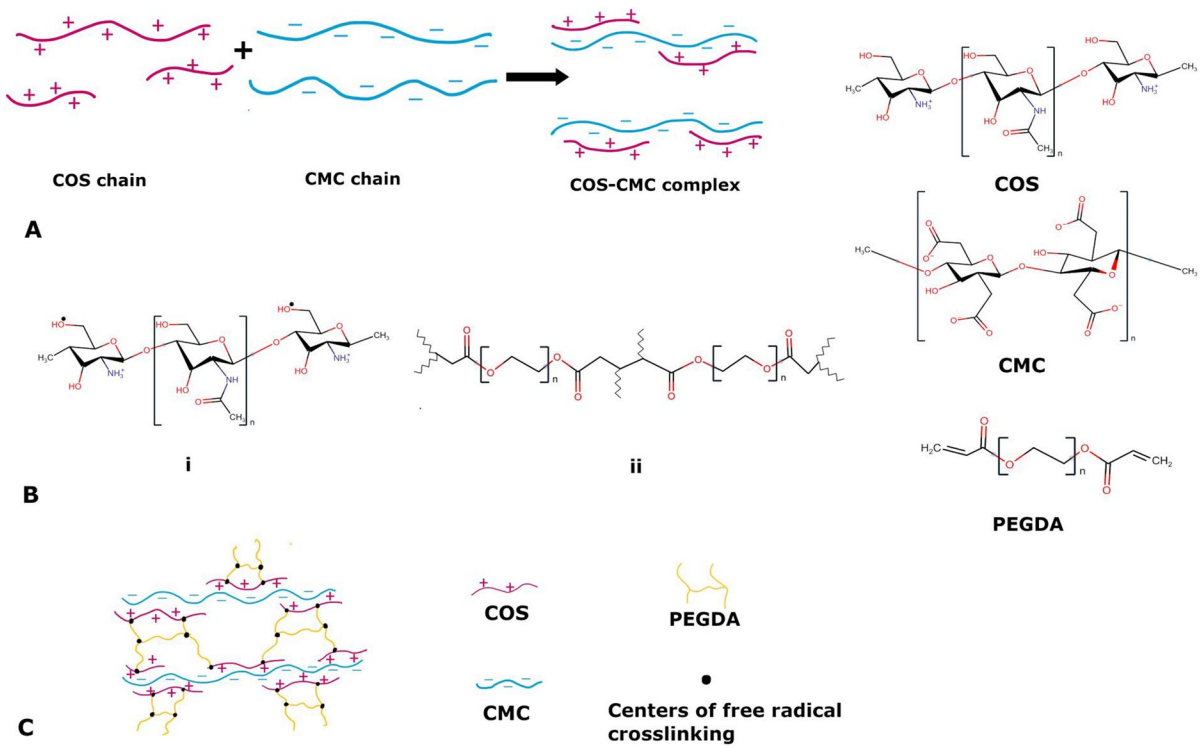

Fig. 6 **A** Poly-ionic complexation between COS and CMC; **B** Radical formation on COS chains (● indicate free radical centers due to UV radiation; wavy lines indicate cross-linking ends of PEGDA, formed after UV irradiation); **C** Poly-ionic COS-CMC complex cross-linked with PEGDA.

material (Ahmed 2015; Hafezi 2019; Li et al. 2015; Tian et al. 2015); in this case, both PEGDA and COS were observed to be soluble in pH 7. Morris et al. determined that COS-PEGDA photopolymerized hydrogels had a swelling ratio of 8 when the COS:PEGDA ratio was 1:5. Such hydrogels were capable for use as artificial tissue scaffolds (Morris et al. 2017). Chitosan-based hydrogels were found to have swelling ratios ranging from 4 to 8 in previous studies (Yao et al. 2019; Zhou et al. 2011). High water swelling ratios improve the water retention capability of the hydrogel and are related to larger mesh sizes in the gel network, thus allowing enhanced cell proliferation due to effective nutrient diffusion into the network (Park et al. 2009). Swelling ratio depends on several factors, such as the concentration of the precursor polymers, crosslinker and photoinitiator, as well as the extent of crosslinking (Slaughter et al. 2009).

Hydrogel morphology

SEM micrographs of the hydrogel cross-sections revealed irregular porous networks in both gels (Fig. 7). However, the pores in COSPCMC-2 were sparse, but of definite shapes. The surfaces also appeared to be smooth. COSPCMC-4 exhibited a highly irregular interconnected macroporous network and a rough texture (Fig. 7B). Such textures have previously been observed in COS-PEGDA hydrogels prepared via photopolymerization (Morris et al. 2017; Muñoz and Zuluaga 2017). It is possible that the increased CMC content in COSPCMC-4 interfered with the crosslinking between COS and PEGDA chains, as previous studies have found that presence of CMC in PEGDA hydrogels resulted in such textures (He et al. 2017; Kono 2014). The loosely packed network also explained why this hydrogel exhibited better swelling. Due to the superior swelling capacity

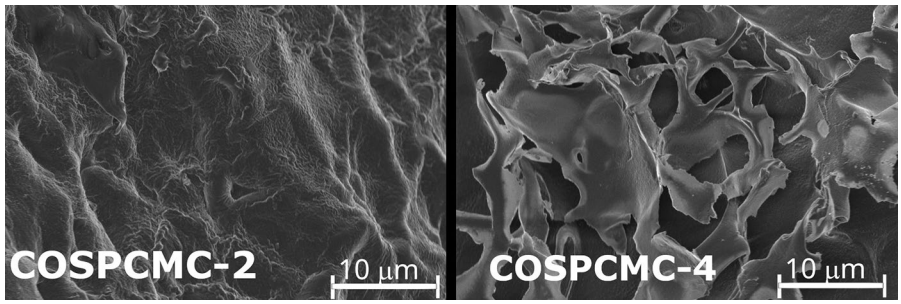

Fig. 7 SEM images of the cross-sections of the two hydrogels; **a** COSPCMC-2 (containing 2% CMC), **b** COSPCMC-4 (containing 4% CMC). Pores have been marked inside white boxes. Images at a magnification of 5 kX

and porous structure of COSPCMC-4, it was chosen for subsequent analyses.

Functional group analysis

FTIR spectra of the two hydrogels (after washing in PBS buffer and freeze-drying) revealed important characteristic peaks (Fig. S3), which are summarized in Table S4. The peaks were identified using the peak analyzer feature of the OMICS Spectral Analysis Software. After interpretation of the peaks, the presence of all three polymers in the hydrogel could be ascertained, which implied that cross-linking was successful.

Cytotoxicity assays

The use of photoinitiators (Irgacure 2959) and synthetic polymers such as PEGDA increase the risk of cytotoxicity of hydrogels. In addition to the toxicity of the hydrogel itself, a concern in biomedical applications is the possibility of chemicals leaching from the hydrogel. Cytotoxicity studies conducted on Vero cells revealed that the leach-out products were not cytotoxic to any extent, as the cell viability was more than 95% (Fig. 8).

Mechanical tests

Uniaxial compression tests of COSPCMC-4 under swollen conditions and room temperature revealed that the material failed at forces above 0.2–1.8 N. The curves shown are representative of one sample. The stress against λ-λ^{-2} curve (which is associated with the shear strain) (Fig. 9) is similar to those obtained for cross-linked materials experimentally (Anseth et al. 1996; Muniz and Geuskens 2001). It can be seen that the curve exhibited non-linear characteristics, which is indicative of the viscoelastic behavior of hydrogels, that is a resistance to shear stress while maintaining elastic deformability (Anseth et al. 1996). The viscosity is a result of the free water and amorphous regions (Li et al. 2016). The curve exhibited small slopes at low deformations, as the surface of the sample was not perfectly flat. Curve fitting in the linear portion of the graphs was used to evaluate the compressive modulus, which was 4.5 ± 2.7 kPa ($n = 3$, $\pm$S.D). Such elasticities are ten-fold lower than soft skeletal muscles (25 kPa) (Mathur et al. 2001). Banerjee et al. developed alginate hydrogels for the encapsulation of neural stem cells that mimicked soft neural tissues. The elastic modulus values were in the range 0.18-20 kPa; however, brain tissues have a

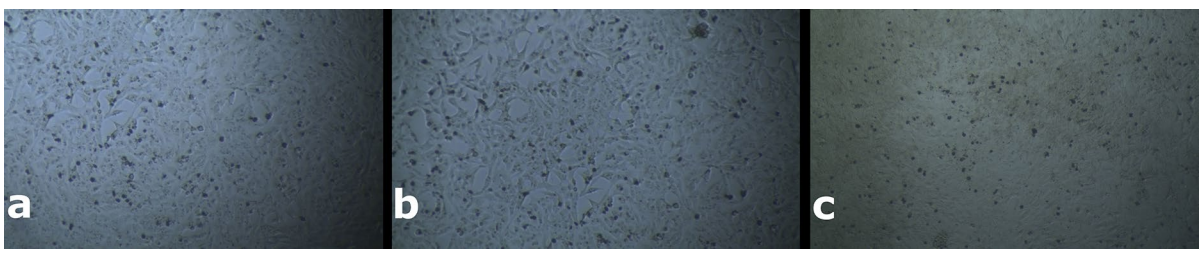

Fig. 8 Vero cells observed under an optical microscope. **a** With leachant solution from 2.5 mg/mL hydrogel, **b** With leachant solution from 5 mg/mL hydrogel, **c** With leachant solution from 10 mg/mL hydrogel

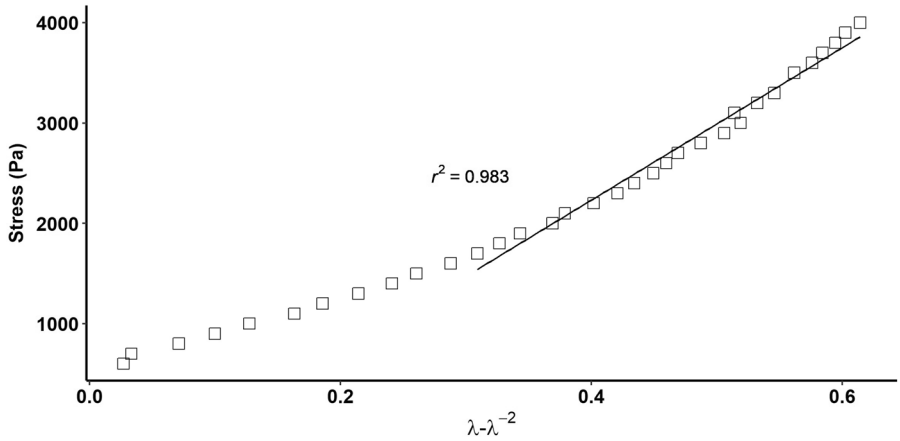

Fig. 9 Compressive stress as a function of $\lambda - \lambda^{-2}$. Regression line of best fit in the linear portion of the graph was used to evaluate Young's modulus

modulus range of 100–1000 Pa, and as such, hydrogels having an elastic modulus of 180 Pa effectively promoted neuronal differentiation (Banerjee et al. 2009). Saha et al. determined that glial cell (responsible for brain structure, plasticity and nerve functions) differentiation was higher when hydrogel elastic modulus was of the range 1–10 kPa (Saha et al. 2008). In fibrin hydrogels, when the Young's modulus was 30 kPa, Chondrocyte differentiation was the highest, in addition to type II collagen levels (Bachmann et al. 2020). It can thus be inferred that the stiffness of the gels must be such that it supports the activity of the cells for which it has been designed. Nevertheless, additional reinforcement using other polymers or improved cross-linking should be considered for COSPCMC-4 to increase the modulus to levels that are strong enough for in vivo use as artificial scaffolds (Morris et al. 2017).

Conclusion

Despite the numerous applications and benefits of COS, the main deterrent in its use is the lack of convenient production techniques. This work was intended to fill a critical research gap and develop a facile method for chitosan depolymerization. To test the applicability of the COS, a biocompatible hydrogel was developed. Among several different processing routes, physicochemical methods were found to be the most well-characterized and convenient. In this study, the ease and efficiency of irradiating a solid powder was taken into consideration and a two-stage method was devised, where gamma radiation would precede oxidative degradation with hydrogen peroxide. Several combinations of reaction conditions were tested to optimize the process so that dose level, temperature of H_2O_2 reaction and the concentration of the peroxide itself would be minimum. We determined that irradiation at 15 kGy, followed by oxidative degradation at 2% H_2O_2, at 25^0 C in an overnight reaction yielded COS that was soluble in pH 7–8. MW was reduced by 95%, from 249 to 12.8 ± 1.6 kDa, while DD was found to be 62.3%. Physical and chemical characterization revealed that the precursor chitosan was depolymerized, yet its functional groups remained unchanged in the process. This ascertained that the depolymerization process was suitable for COS that could be used subsequently, and a photopolymerized hydrogel was developed. The hydrogel exhibited high porosity and swelling ratios (6.44–7.17), comparable to those designed for tissue engineering and the compressive modulus was 4.5 ± 2.7 kPa, similar to that of soft tissues. Thus, the viability of COS in hydrogels was proven through the experiment. In addition of COS biomedical applications, we anticipate this newly developed hydrogel could be a potential candidate for the production of 3D printable bioink suitable for soft tissue engineering.

Acknowledgments The authors wish to thank the Institute of Food and Radiation Biology, Atomic Energy Commission, Savar, Dhaka for conducting the gamma irradiation, the Center for Advanced Research in Sciences, Dhaka and the Atomic Energy Research Center, Dhaka and the Department of Chemistry, BUET for providing the facilities for the characterization studies.

Author contributions NT: Conceptualization, Methodology, Data curation, Formal analysis, Investigation, Validation, Visualization, Writing – original draft, Writing – review; SA: Conceptualization, Methodology, Resources, Writing – Review & Editing, Supervision, Project administration, Funding acquisition; MMI and R-U-H: Investigation; MAA: Conceptualization, Methodology, Resources, Writing – Review & Editing, Supervision.

Funding Open Access funding enabled and organized by CAUL and its Member Institutions. This research did not receive any specific grant from funding agencies in the public, commercial, or not-for-profit sectors.

Declarations

Conflict of interest none.

References

Abd El-Rehim HA, Zahran DA, El-Sawy NM, Hegazy ES (2015) Gamma irradiated Chitosan and its derivatives as antioxidants for minced chicken. Biosci Biotechnol Biochem 79(6):997–1004. https://doi.org/10.1080/09168451.2014.997187

Ahmed EM (2015) Hydrogel: preparation, characterization, and applications: a review. J Adv Res 6(2):105–121. https://doi.org/10.1016/j.jare.2013.07.006

Anseth KS, Bowman CN, Lisa B-P (1996) Mechanical properties of hydrogels and their experimental determination. Biomaterials 17(17):1647–1657. https://doi.org/10.1016/0142-9612(96)87644-7

Bachmann B, Spitz S, Schädl B, Teuschl AH, Redl H, Nürnberger S, Ertl P (2020) Stiffness matters: fine-tuned hydrogel elasticity alters chondrogenic redifferentiation. Front Bioeng Biotechnol. https://doi.org/10.3389/fbioe.2020.00373

Banerjee A, Arha M, Choudhary S, Ashton RS, Surita R, Bhatia DV, Schaffer, Kane RS (2009) The influence of hydrogel Modulus on the proliferation and differentiation of encapsulated neural stem cells. Biomaterials 30(27):4695–4699. https://doi.org/10.1016/j.biomaterials.2009.05.050

Barbucci R, Magnani A, Consumi M (2000) Swelling behavior of carboxymethylcellulose hydrogels in relation to cross-linking, PH, and charge density. Macromolecules 33(20):7475–7480. https://doi.org/10.1021/ma0007029

Bernardino-Nicanor A, Acosta-García G, Güemes-Vera N, Montañez-Soto JL, de los Ángeles Vivar-Vera M, González-Cruz L (2017) Fourier transform infrared and Raman spectroscopic study of the effect of the thermal treatment and extraction methods on the characteristics of ayocote bean starches. J Food Sci Technol 54(4):933–943. https://doi.org/10.1007/s13197-016-2370-1

Brugnerotto J, Lizardi J, Goycoolea FM, Argüelles-Monal W, J Desbrières, and, Rinaudo M (2001) An Infrared Investigation in Relation with Chitin and Chitosan characterization. Polymer 42(8):3569–3580. https://doi.org/10.1016/S0032-3861(00)00713-8

Cabrera JC (2005) Preparation of chitooligosaccharides with degree of polymerization higher than 6 by acid or enzymatic degradation of Chitosan. Biochem Eng J 25(2):165–172. https://doi.org/10.1016/j.bej.2005.04.025

Capanema NS, Mansur AA, de Jesus AC, Carvalho SM, de Oliveira LC, Mansur HS (2018) Superabsorbent crosslinked carboxymethyl cellulose-PEG hydrogels for potential wound dressing applications. Int J Biol Macromol 106(January):1218–1234. https://doi.org/10.1016/j.ijbiomac.2017.08.124

Chae SY, Jang MK, Nah JW (2005) Influence of molecular weight on oral absorption of water soluble Chitosans. J Controlled Release 102(2):383–394. https://doi.org/10.1016/j.jconrel.2004.10.012

Chang KLB, Tai MC, Cheng FH (2001) Kinetics and products of the degradation of Chitosan by hydrogen peroxide. J Agric Food Chem 49(10):4845–4851. https://doi.org/10.1021/jf001469g

Chen Y-M, Chung Y-C, Wang LW, Chen K-T, Li S-Y (2002) Antibacterial properties of Chitosan in waterborne pathogen. J Environ Sci Health Part A 37(7):1379–1390

Chesnutt BM, Viano AM, Yuan Y, Yang Y, Guda T, Appleford MR, Ong JL, Haggard WO, Bumgardner JD (2009) Design and characterization of a novel Chitosan/nanocrystalline calcium phosphate composite scaffold for bone regeneration. J Biomedical Mater Res Part A 88A(2):491–502. https://doi.org/10.1002/jbm.a.31878

Choi W-S, Ahn K-J, Lee D-W, Byun M-W (2002) Preparation of Chitosan oligomers by irradiation. Polym Degrad Stab 78(3):533–538. https://doi.org/10.1016/S0141-3910(02)00226-4

Dong Y, Xu C, Wang J, Wang M, Wu Y (2001) Determination of degree of substitution for N-acylated Chitosan using IR spectra. Sci China Ser B Chem 44(2):216–224. https://doi.org/10.1007/BF02879541

Duy NN, Van Phu D, Anh NT, Hien NQ (2011) Synergistic degradation to prepare oligochitosan by γ-irradiation of Chitosan solution in the presence of hydrogen peroxide. Radiat Phys Chem 80(7):848–853. https://doi.org/10.1016/j.radphyschem.2011.03.012

Fan M (2009) Preparation and structure of Chitosan soluble in wide PH range. Carbohydr Polym 78(1):66–71. https://doi.org/10.1016/j.carbpol.2009.03.031

Fan H, Vitharana SN, Chen T, O'Keefe D, Middaugh CR (2007) Effects of PH and polyanions on the thermal stability of fibroblast growth factor 20. Mol Pharm 4(2):232–240. https://doi.org/10.1021/mp060097h

Fekete T, Borsa J, Takács E (2017) Synthesis of carboxymethylcellulose/starch superabsorbent hydrogels by gamma-irradiation. Chem Cent J 11:46. https://doi.org/10.1186/s13065-017-0273-5

García MA, de la Paz N, Castro C, Rodríguez JL, Rapado M, Zuluaga R, Ganán P, Casariego A (2015) Effect of molecular weight reduction by gamma irradiation on the antioxidant capacity of Chitosan from lobster shells. J Radiat Res Appl Sci 8(2):190–200. https://doi.org/10.1016/j.jrras.2015.01.003

Hafezi F (2019) 3D printed Chitosan dressing crosslinked with Genipin for potential healing of chronic wounds. Int J Pharm 506:406

Hai L, Diep TB, Nagasawa N, Yoshii F, Kume Tamikazu (2003) Radiation depolymerization of Chitosan to prepare oligomers. Nuclear Instrum Methods Phys Res Sect B Beam Interacti Mater Atoms 208(August):466–470. https://doi.org/10.1016/S0168-583X(03)01181-9

Harish Prashanth KV, Tharanathan RN (2007) Chitin/Chitosan: modifications and their unlimited application potential—an overview. Trends Food Sci Technol 18(3):117–131. https://doi.org/10.1016/j.tifs.2006.10.022

He T, Wu D, Wang X, Rong J, Zhao J (2017) Photo-Crosslinking Hyaluronan-Heparin hybrid hydrogels for BMP-2 sustained delivery. J Polym Eng 37(2):125–133. https://doi.org/10.1515/polyeng-2015-0379

Hien NQ, Van Phu D, Duy NN, Lan NTK (2012) Degradation of Chitosan in solution by gamma irradiation in the presence of hydrogen peroxide. Carbohydr Polym 87(1):935–938. https://doi.org/10.1016/j.carbpol.2011.08.018

Jiang Z, Chi J, Li H, Wang Y, Liu W (2021) Effect of Chitosan oligosaccharide-conjugated selenium on improving immune function and blocking gastric cancer growth. Eur J Pharmacol 891(January):173673. https://doi.org/10.1016/j.ejphar.2020.173673

Jin Q, Yu H, Wang X, Li K, Li P (2017) Effect of the molecular weight of water-soluble Chitosan on its fat-/cholesterol-binding capacities and inhibitory activities to pancreatic lipase. PeerJ 5(May):e3279. https://doi.org/10.7717/peerj.3279

Jung S (2012) Fabrication of Chitosan-poly(ethylene glycol) hybrid hydrogel microparticles via replica molding and its application toward facile conjugation of biomolecules. Langmuir 28(49):17061–17070. https://doi.org/10.1021/la303567p

Kabal'Nova NN, Murinov KYu, Mullagaliev IR, Krasnogorskaya NN, Shereshovets VV, Monakov YuB, Zaikov GE (2001) Oxidative destruction of Chitosan under the effect of ozone and hydrogen peroxide. J Appl Polym Sci 81(4):875–881. https://doi.org/10.1002/app.1506

Kazami N, Sakaguchi M, Mizutani D, Masuda T, Wakita S, Oyama F, Kawakita M, Sugahara Y (2015) A simple procedure for preparing Chitin oligomers through acetone precipitation after hydrolysis in concentrated hydrochloric acid. Carbohydr Polym 132(November):304–310. https://doi.org/10.1016/j.carbpol.2015.05.082

Kim S (2005) Enzymatic production and biological activities of Chitosan oligosaccharides (COS): a review. Carbohydr Polym 62(4):357–368. https://doi.org/10.1016/j.carbpol.2005.08.012

Kim M-O, Moon D-O, Kang C-H, Choi YH, Lee J-D (2013) Water-soluble Chitosan sensitizes apoptosis in human leukemia cells via the downregulation of Bcl-2 and dephosphorylation of akt. J Food Biochem 37(3):270–277. https://doi.org/10.1111/j.1745-4514.2011.00628.x

Kittur FS, Harish Prashanth KV, Udaya Sankar K, Tharanathan RN (2002) Characterization of chitin, Chitosan and their carboxymethyl derivatives by differential scanning calorimetry. Carbohydr Polym 49(2):185–193. https://doi.org/10.1016/S0144-8617(01)00320-4

Kono H (2014) Characterization and properties of carboxymethyl cellulose hydrogels crosslinked by polyethylene glycol. Carbohydr Polym 106:84–93. https://doi.org/10.1016/j.carbpol.2014.02.020

Li B, Wang L, Xu F, Gang X, Demirci U, Wei D, Li Y, Feng Y, Jia D (2015) Hydrosoluble, UV-crosslinkable and injectable Chitosan for patterned cell-laden microgel and rapid transdermal curing hydrogel in vivo. Acta Biomater 22(August):59–69. https://doi.org/10.1016/j.actbio.2015.04.026

Li W, Wang D, Yang W (2016) Compressive mechanical properties and microstructure of PVA–HA hydrogels for cartilage repair. RSC Adv 6(24):20166–20172. https://doi.org/10.1039/C6RA02166B

Liaqat F (2018) Chitooligosaccharides and their biological activities: a comprehensive review. Carbohydr Polym 184(March):243–259. https://doi.org/10.1016/j.carbpol.2017.12.067

Lin C-W, Lin J-C (2003) Characterization and blood coagulation evaluation of the water-soluble chitooligosaccharides prepared by a facile fractionation method. Biomacromolecules 4(6):1691–1697. https://doi.org/10.1021/bm034129n

Lin L, Wang Y, Wang L, Pan J, Xu Y, Li S, Huang D et al (2020) Injectable microfluidic hydrogel microspheres based on Chitosan and poly(ethylene glycol) diacrylate (PEGDA) as chondrocyte carriers. RSC Adv 10(65):39662–39672. https://doi.org/10.1039/D0RA07318K

Liu H, Tao WM, Li G, Xu XY, Li XF, Bai P, Wei C, Yu GD (2009) Chitosan oligosaccharides attenuate hydrogen peroxide-induced stress injury in human umbilical vein endothelial cells. Pharmacol Res 59(3):167–175. https://doi.org/10.1016/j.phrs.2008.12.001

Lopatin SA, Derbeneva M, Kulikov S, Varlamov V (2009) Fractionation of Chitosan by ultrafiltration. J Anal Chem J Anal Chem Eng 64(June):648–651. https://doi.org/10.1134/S1061934809060197

Mallakuntla MK, Penugurti V, Manavathi B, Podile AR (2021) Chitooligosaccharides induce apoptosis in human breast cancer cells. Carbohydr Polym Technol Appl 2:100077. https://doi.org/10.1016/j.carpta.2021.100077

Mathur AB, Collinsworth AM, Reichert WM, Kraus WE, Truskey GA (2001) Endothelial, cardiac muscle and skeletal muscle exhibit different viscous and elastic properties as determined by atomic force microscopy. J Biomech

34(12):1545–1553. https://doi.org/10.1016/S0021-9290(01)00149-X

Mendis E, Kim M-M, Rajapakse N (2007) An in vitro cellular analysis of the radical scavenging efficacy of chitooligosaccharides. Life Sci 80(23):2118–2127. https://doi.org/10.1016/j.lfs.2007.03.016

Mengíbar M, Mateos-Aparicio I, Miralles B, Heras Á (2013) Influence of the physico-chemical characteristics of chitooligosaccharides (COS) on antioxidant activity. Carbohydr Polym 97(2):776–782. https://doi.org/10.1016/j.carbpol.2013.05.035

Morris VB, Nimbalkar S, Younesi M, McClellan P (2017) Mechanical properties, cytocompatibility and manufacturability of Chitosan: PEGDA hybrid-gel scaffolds by stereolithography. Ann Biomed Eng 45(1):286–296. https://doi.org/10.1007/s10439-016-1643-1

Mourya VK, Inamdar NN, Choudhari YM (2011) Chitooligosaccharides: synthesis, characterization and applications. Polym Sci Ser A 53:583–612. https://doi.org/10.1134/S0965545X11070066

Muanprasat C (2017) Chitosan oligosaccharide: biological activities and potential therapeutic applications. Pharmacol Ther 170(February):80–97. https://doi.org/10.1016/j.pharmthera.2016.10.013

Muley AB, Ladole MR, Suprasanna P, Dalvi SG (2019) Intensification in biological properties of Chitosan after γ-irradiation. Int J Biol Macromol 131:435–444. https://doi.org/10.1016/j.ijbiomac.2019a.03.072

Muley AB, Shingote PR, Patil AP, Dalvi SG, Suprasanna P (2019) Gamma radiation degradation of Chitosan for application in growth promotion and induction of stress tolerance in potato (*Solanum Tuberosum* L). Carbohydr Polym 210(April):289–301.

Muniz EC, Geuskens G (2001) Compressive elastic Modulus of polyacrylamide hydrogels and semi-IPNs with poly(N-isopropylacrylamide). Macromolecules 34(13):4480–4484. https://doi.org/10.1021/ma001192l

Najafabadi SA, Ayati H, Honarkar M, Moghadam V, Mirkhani M, Tahriri, Tayebi L (2018) UV Irradiation-H_2O_2 system as an effective combined depolymerization technique to produce oligosaccharides from Chitosan. Bio-Des Manuf 1(1):62–68. https://doi.org/10.1007/s42242-018-0005-2

Naqvi S (2017) The cell factory approach toward biotechnological production of high-value Chitosan oligomers and their derivatives: an update. Crit Rev Biotechnol 37(1):11–25. https://doi.org/10.3109/07388551.2015.1104289

Nguyen N, Thuy DQ, Hoang ND, Nguyen QH, Nguyen DS (2017) Preparation, characterization, and antioxidant activity of water-soluble oligochitosan. Green Process Synthesis 6(5):461–468. https://doi.org/10.1515/gps-2016-0126

MR Paneque, AA Valentín, DS Vidal, C Wandrey (2004) Physical-chemical modification of Sodium Alginate ALGIMAR by Irradiation. Nucleus 35:55–59

Park P-J, Je J-Y (2003) Free radical scavenging activity of chitooligosaccharides by electron spin resonance spectrometry. J Agric Food Chem 51(16):4624–4627. https://doi.org/10.1021/jf034039+

Park H, Guo X, Temenoff JS, Tabata Y, Caplan AI, Kasper FK, Mikos AG (2009) Effect of swelling ratio of injectable hydrogel composites on chondrogenic differentiation of encapsulated rabbit marrow mesenchymal stem cells in vitro. Biomacromolecules 10(3):541–546. https://doi.org/10.1021/bm801197m

Peppas NA, Catherine TR (1983) Solute diffusion in Swollen membranes. Part I. A new theory. J Membr Sci 15(3):275–287. https://doi.org/10.1016/S0376-7388(00)82304-2

Qin CQ, Du YM, Xiao L (2002) Effect of hydrogen peroxide treatment on the molecular weight and structure of Chitosan. Polym Degrad Stab 76(2):211–218. https://doi.org/10.1016/S0141-3910(02)00016-2

Reeves R, Ribeiro A, Lombardo L, Boyer R, Leach JB (2010) Synthesis and characterization of carboxymethylcellulose-methacrylate hydrogel cell scaffolds. Polymers 2(3):252–264. https://doi.org/10.3390/polym2030252

Saha K, Keung AJ, Irwin EF, Li Y, Little L, Schaffer DV (2008) Substrate modulus directs neural stem cell behavior. Biophys J 95(9):4426–4438. https://doi.org/10.1529/biophysj.108.132217

Samuels RJ (1981) Solid state characterization of the structure of Chitosan films. J Polym Sci Polym Phys Ed 19(7):1081–1105

Sato K, Saimoto H, Morimoto M, Shigemasa Y (2003) Depolymerization of chitin and Chitosan under hydrothermal conditions. Sen-I Gakkaishi 59(3):104–109

Savitri E, Sumarno S (2015) Degradation of Chitosan by hydrothermal process in the presence of sonication pretreatment with supercritical CO_2 as pressurized fluid. Macromol Sympos 353:212–219. https://doi.org/10.1002/masy.201550329

Shorrock CJ, Rees WD (1988) Overview of gastroduodenal mucosal protection. Am J Med 84(2A):25–34. https://doi.org/10.1016/0002-9343(88)90251-3

Slaughter BV, Khurshid SS, Fisher OZ, Khademhosseini A, Peppas NA (2009) Hydrogels in regenerative medicine. Adv Mater 21:3307–3329. https://doi.org/10.1002/adma.200802106

Tian F, Keao YL, Zhao B (2003) The depolymerization mechanism of Chitosan by hydrogen peroxide. J Mater Sci 38(23):4709–4712. https://doi.org/10.1023/A:1027466716950

Tian M, Tan H, Li H, You C (2015) Molecular weight dependence of structure and properties of Chitosan oligomers. RSC Adv 5(85):69445–69452. https://doi.org/10.1039/C5RA08358C

Timur M, Paşa A (2018) Synthesis, characterization, swelling, and metal uptake studies of aryl cross-linked Chitosan hydrogels. ACS Omega 3(12):17416–17424. https://doi.org/10.1021/acsomega.8b01872

Tomida H, Fujii T, Furutani N, Michihara A, Yasufuku T, Akasaki K, Maruyama T, Otagiri M, Gebicki JM (2009) Antioxidant properties of some different molecular weight Chitosans. Carbohydr Res 344(13):1690–1696. https://doi.org/10.1016/j.carres.2009.05.006

Trombotto S, Ladavière C, Delolme F (2008) Chemical Preparation and Structural characterization of a homogeneous series of Chitin/Chitosan oligomers. Biomacromolecules 9(7):1731–1738. https://doi.org/10.1021/bm800157x

Vo T-S, Kong C-S, Kim S-K (2011) Inhibitory effects of chitooligosaccharides on degranulation and cytokine generation in rat basophilic leukemia RBL-2H3 cells. Carbohydr

Polym 84(1):649–655. https://doi.org/10.1016/j.carbpol.2010.12.046

Wang W, Bo S, Li S (1991) Determination of the Mark-Houwink equation for Chitosans with different degrees of deacetylation. Int J Biol Macromol 13(5):281–285. https://doi.org/10.1016/0141-8130(91)90027-R

Wu N, Wen Z-S, Xiang X-W, Huang Y-N, Gao Y, Qu YL (2015) Immunostimulative activity of low molecular weight Chitosans in RAW264.7 macrophages. Mar Drugs 13(10):6210–6225. https://doi.org/10.3390/md13106210

Xuan, D and Bui V 2019 Study on Preparation of Water-Soluble Chitosan with Varying Molecular Weights and Its Antioxidant Activity. Advances in Materials Science and Engineering. https://doi.org/10.1155/2019/8781013

Yao H-Y, Lin H-R, Sue G-P, Lin Y-J (2019) Chitosan-based hydrogels prepared by UV polymerization for wound dressing. Polym Polym Compos 27(3):155–167. https://doi.org/10.1177/0967391118820477

Yoksan R, Akashi M, Miyata M (2004) Optimal γ-ray dose and irradiation conditions for producing low-molecular-weight Chitosan that retains its chemical structure. Radiat Res 161(4):471–480. https://doi.org/10.1667/RR3125

Zainol I, Akil HM (2009) Effect of γ-irradiation on the physical and mechanical properties of Chitosan powder. Mater Sci Eng C 29(1):292–297. https://doi.org/10.1016/j.msec.2008.06.026

Zhou Y, Ma G, Shi S, Yang D (2011) Photopolymerized water-soluble Chitosan-based hydrogel as potential use in tissue engineering. Int J Biol Macromol 48(3):408–413. https://doi.org/10.1016/j.ijbiomac.2010.12.015

Zhu X, Chen J, Hu Y, Zhang N, Fu Y, Chen X (2021) Tuning complexation of carboxymethyl cellulose/cationic Chitosan to stabilize pickering emulsion for curcumin encapsulation. Food Hydrocolloids 110:106135. https://doi.org/10.1016/j.foodhyd.2020.106135

Zou P, Yang X, Wang J, Li Y, Yu H, Zhang Y (2016) Advances in characterisation and biological activities of Chitosan and Chitosan oligosaccharides. Food Chem 190(12):1174–1181. https://doi.org/10.1016/j.foodchem.2015.06.076

Gao Hao-qi, Xu Liang-feng, Yang Jian-ping, Kai-xun, Chen (2004) "A Study on Degradation of Chitosan in Near-Critical Water and Distributing Orderliness of Products." *Journal of Northwest University (Natural Science Edition)*. http://en.cnki.com.cn/Article_en/CJFDTOTAL-XBDZ200404015.htm

NTHaiNThiTThanhLeTTNgaHoa2019Le Nghiem Anh Tuan, Dang Van Phu, and Nguyen Quoc Hien10.1007/s10924-019-01479-yHai NT, Le Thanh NThiT, Nga TT, Hoa (2019) Preparation of Chitooligosaccharide by Hydrogen Peroxide Degradation of Chitosan and Its Effect on Soybean Seed Germination. J Polym Environ 27(9):2098–2104. https://doi.org/10.1007/s10924-019-01479-y. Le Nghiem Anh Tuan, Dang Van Phu, and Nguyen Quoc Hien

Kang B, Shuquan Chang X-B, Tang Y-D, Dai, Chen D (2007) Study on the water-solubility of Chitosan degraded with gamma radiation 35: 49–52

Muñoz G, and Fabio Zuluaga (2017) Chitosan, Chitosan derivatives and their Biomedical Applications. 87–106. https://doi.org/10.5772/66527

Uchida Y, Izume M, Ohtakara A (1989) Preparation of Chitosan oligomers with purifed chitosanase and its application. In: Chitin and Chitosan: sources, chemistry, biochemistry, physical properties and applications. Elsevier, pp 372–382